Inorganic Chemistry

Article

pubs.acs.org/IC

Spin $^1/_2$ Delafossite Honeycomb Compound Cu_5SbO_6

E. Climent-Pascual,*[,†] P. Norby,[‡] N.H. Andersen,[‡] P.W. Stephens,[§] H.W. Zandbergen,[⊥] J. Larsen,[‡] and R.J. Cava[†,‡]

[†]Department of Chemistry, Princeton University, Princeton, New Jersey 08544, United States

[‡]Materials Research Division, Risø DTU, Technical University of Denmark, DK-4000 Roskilde, Denmark

[§]Department of Physics and Astronomy, Stony Brook University, Stony Brook, New York 11794, United States

[⊥]National Centre for HREM, Delft University of Technology, 2628 CJ Delft, The Netherlands

ABSTRACT: Cu_5SbO_6 is found to have a monoclinic, Delafossite-derived structure consisting of alternating layers of O−Cu(I)−O sticks and magnetic layers of Jahn−Teller distorted $Cu(II)O_6$ octahedra in an edge sharing honeycomb arrangement with $Sb(V)O_6$ octahedra. This yields the structural formula $Cu(I)_3Cu(II)_2Sb(V)O_6$. Variants with ordered and disordered layer stacking are observed, depending on the synthesis conditions. The spin $^1/_2$ Cu^{2+} ions form dimers in the honeycomb layer. The magnetic susceptibility measured between 5 and 300 K is characteristic of the presence of a singlet−triplet spin gap of 189 K. High resolution synchrotron X-ray diffraction studies indicate that changes in the intra- or interdimer distances between 300 and 20 K, such as might indicate an increase in strength of the Peierls-like distortion through the spin gap temperature, if present, are very small. A comparison to the $NaFeO_2$-type Cu^{2+} honeycomb compounds $Na_3Cu_2SbO_6$ and $Na_2Cu_2TeO_6$ is presented.

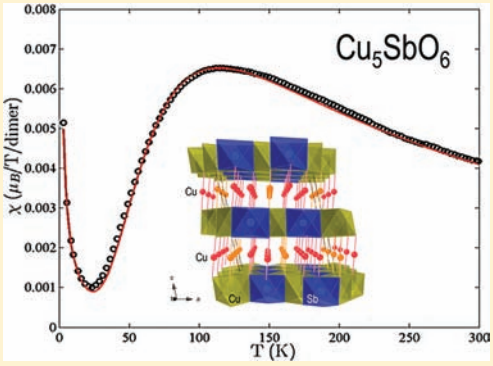

1. INTRODUCTION

Compounds with magnetic ions arranged in 1- or 2-dimensional sublattices continue to be of interest in the study of magnetism, especially in the context of geometric magnetic frustration.[1] Among these, compounds based on Cu^{2+} are especially appealing because at spin $^1/_2$, quantum effects are expected to be important in determining the magnetic properties. Recent observations of the properties of mineral-based cuprates[2,3] based on kagome lattices are of particular interest in this regard. Although not generally appreciated to be frustrated, magnetic ions on honeycomb lattices frequently display nontrivial types of magnetic ordering at low temperatures because of frustration that arises from the presence of strong competition between nearest neighbor and second nearest neighbor magnetic interactions.[4,5] The Jahn−Teller distortion for $3d^9$ Cu^{2+} frequently prevents the formation of ideal magnetic lattice geometries, and, in the case of the two honeycomb layer cuprates known, $NaFeO_2$-derived $Na_3Cu_2SbO_6$ and $Na_2Cu_2TeO_6$,[6,7] results in the presence of strong $S = 0$ Cu−Cu dimers across a subset of the shared edges of the octahedra in the honeycomb plane.

A compound variously reported as having composition Cu_5SbO_6 or $Cu_4SbO_{4.5}$ is known to occur in the Cu−Sb−O chemical system,[8−11] but its crystal structure and magnetic properties have not previously been reported. Here we show that the compound has the formula Cu_5SbO_6 and has a Delafossite-derived structure, with planes of O−Cu(I)−O sticks alternating with planes of edge sharing MO_6 octahedra; the ordering of Cu^{2+} and Sb^{5+} octahedra in a 2:1 ratio results in a honeycomb geometry for the Cu ions and leads to a triple Delafossite formula unit; octahedral distortions and shifts in the stacking of neighboring planes lead to monoclinic symmetry. Similar structures are found for other Delafossite honeycomb compounds either synthesized directly or via ion exchange from $NaFeO_2$-derived starting materials.[12−14] We find that the plane stacking in Cu_5SbO_6 can be regular or disordered, with the disordered stacking variant stable on synthesis at 1000 °C, and the ordered stacking variant favored just below the melting point of 1160 °C in air. Overall monoclinic symmetry and disordered stacking are commonly found in $NaFeO_2$-type derivatives with triangular and honeycomb magnetic layers;[15−17] we do not observe the 3R versus 2H polytypism frequently seen in Delafossites.[18,19] Our magnetic characterization shows Cu_5SbO_6 to display a singlet−triplet gap of ∼189 K, which we attribute to the presence of the Cu−Cu dimers in the honeycomb layers. Our structural studies show that the dimerization is weaker than is seen in the previously known Cu honeycomb compounds $Na_3Cu_2SbO_6$ and $Na_2Cu_2TeO_6$, and we therefore studied the crystal structure by high resolution synchrotron X-ray diffraction at 20 K and ambient temperature, to determine whether the dimerization increases in strength on cooling, that is, whether there is significant magnetostructural coupling as the spins localize in the $S = 0$ state at low temperatures. No enhancement of the structural dimerization because of the spin singlet formation is observed.

Received: September 21, 2011
Published: December 15, 2011

   dx.doi.org/10.1021/ic202066n | *Inorg. Chem.* 2012, 51, 557−565

2. EXPERIMENTAL SECTION

Synthesis. Samples were prepared by conventional solid state methods. High purity CuO (Alfa Inorganics, 99.99%) and Sb_2O_5 (Alfa Inorganics, 99.9%) were intimately mixed, in a stoichiometric ratio to yield 5Cu:1Sb, and placed in high purity alumina crucibles. Samples were then heated in air to 950 at 100 °C per hour, held for 16 h, cooled, reground, and then pelletized and reheated in air at 1000 °C for 24 h to yield the disordered stacking variant of the phase. The disordered stacking variant was obtained on heating to temperatures up to about 1130 °C above which temperature the ordered stacking variant is found. The most highly crystallized sample of the ordered stacking variant, with the smallest amount of disordered stacking present, was obtained from a sample with an excess of 3 wt % of CuO, with the same heating and soaking cycle, but then cooled at 5 °C per hour to 1040 °C before turning off the furnace. Variation of the composition indicated that single phase samples of the Delafossite honeycomb structure phase could be obtained only for a 5:1 ratio of Cu:Sb.

Characterization Techniques. The reactions were monitored in the laboratory by X-ray powder diffraction (XRPD) using Philips Panalytical X'Pert MPD (Cu $K_{\alpha 1}$) and Bruker D8 FOCUS (Cu $K_{\alpha 1,2}$) diffractometers. High resolution XRPD data for structure analysis were taken at beamline X16C at the National Synchrotron Light Source at Brookhaven National Laboratory. The samples for the high resolution studies were loaded in a glass capillary (ϕ = 0.3 mm) and/or on a plate, and diffraction patterns ($\lambda \approx 0.69889$ Å) were collected for the low temperature and high temperature variants at both 20 and 300 K. Indexing of the powder pattern was performed by means of the successive dichotomy method[20] with the *DICVOL* program.[21] The possible space groups were found from systematic extinctions, and the structure for the ordered Cu_5SbO_6 variant was solved by direct-space methods using the FOX program[22] and refined by the Rietveld method using the FullProf program integrated within the FullProf Suite of programs.[23] Diffraction maxima were fit with the Thompson–Cox–Hastings pseudo-Voigt function, and the background was defined using linear interpolation between a set of fixed points. Simulation of the stacking disorder–order was performed with DIFFaX.[24] This allows for calculation of the powder diffraction pattern based on rigid layer-like building blocks and corresponding stacking operators. For this simulation, the structure of a single building block was taken from the result of the Rietveld refinement of the ordered variant. Electron microscopy was performed on an aberration corrected ($C_S \sim 0$) TITAN high-resolution transmission electron microscope operating at 300 kV. Thin areas were obtained by gently dry crushing the specimens and next making a suspension with ethanol and depositing a few drops on a holey carbon Cu grid.

Magnetic susceptibility measurements were performed by vibrating sample magnetometry (VSM) in a CRYOGENIC cryogen free measurement system (CFMS) with a base temperature of 1.6 K, 16 T maximum magnetic field, and sensitivity of 10^{-6} emu. Polycrystalline sample powders of 300 mg approximate weight were employed. Specific heat measurements were performed by the heat-relaxation method in the temperature range between 2 and 250 K using a Quantum Design physical property measurement system (PPMS). The sample was fixed to the sapphire platform of the sample holder by a small amount of Apiezon grease. The specific heat of the sample holder and the grease was measured separately under the same conditions, and this addendum was subtracted from the experimental values to obtain the specific heat of the ordered variant of Cu_5SbO_6. To subtract the phonon contribution to the specific heat a reference sample of the nonmagnetic structural/chemical analogue $Cu_3Zn_2SbO_6$ was used.[12] Electron Paramagnetic Resonance (EPR) spectra were obtained at 4 K with the samples placed in 4-mm-o.d. quartz tubes in a Bruker EMX spectrometer operating in the X-band utilizing microwave frequencies around 9.5 GHz. The determination of the *g* values was made through the use of the simulation program SimFonia provided with the Bruker EMX EPR spectrometer.

3. RESULTS AND DISCUSSION

Crystal Structure. Representative regions of the XRPD patterns at 300 K for disordered (upper panel) and (lower panel) ordered Cu_5SbO_6 are presented in Figure 1. The fact

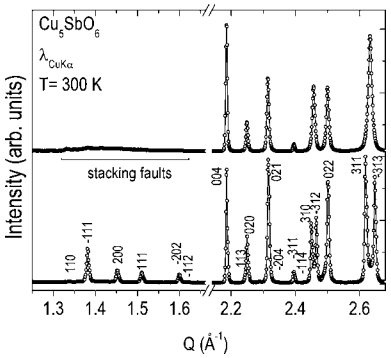

Figure 1. Selected regions of the XRPD (Cu $K_{\alpha 1}$) patterns at 300 K for disordered (upper panel) and ordered (lower panel) variants of Cu_5SbO_6. The patterns are clearly related, though the differences are significant. A broad peak in the disordered form near Q = 2.64 $Å^{-1}$ splits into two narrow peaks, and peaks at lower Q, in the region 1.3–1.6 $Å^{-1}$ are clearly present in the ordered form but are broadened, weaker, and display an asymmetric shape in the disordered form. The indexing of the diffraction lines for the ordered variant is based on a monoclinic cell $a \sim 8.93$ Å, $b \sim 5.60$ Å, $c \sim 11.85$ Å, and $\beta = 103.6°$.

that the two forms are strongly related can be seen by simple visual comparison. The indexing of the diffraction peaks for the ordered variant, based on the monoclinic cell of $a \sim 8.93$ Å, $b \sim 5.60$ Å, $c \sim 11.85$ Å, and $\beta = 103.6°$, is shown in the lower panel. Two important features can be seen indicating that the two forms are related, although they display differences in the perfection of the stacking of the honeycomb layers. First, the disordered variant displays some peaks that are broader than those in the ordered form (e.g., the peaks near Q = 2.63 $Å^{-1}$), while others (e.g., the peak indexed as the (004) near Q = 2.18 $Å^{-1}$) are equally sharp. Second, there is a low angle region for which a broad feature is seen in the diffraction pattern for the disordered variant (for Q between 1.3 and 1.6 $Å^{-1}$, marked as "stacking faults") whereas distinct peaks are observed in this region for the ordered variant. This anisotropic diffraction peak broadening led us to study the two variants by selected area electron diffraction (SAED). The results of this study are seen in Figure 2, which shows [010] SAED patterns for the disordered

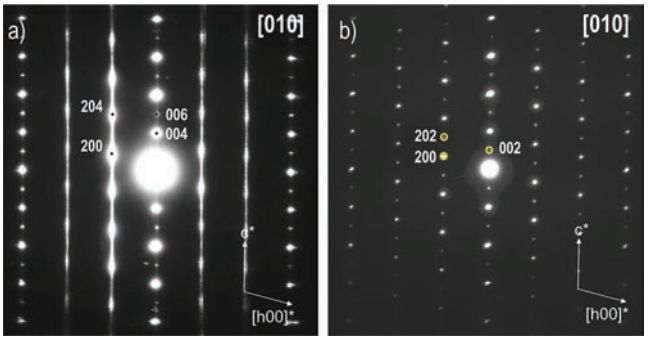

Figure 2. SAED patterns in the [010] reciprocal lattice plane for the disordered (a) and ordered (b) variants of Cu_5SbO_6. The stacking direction is vertical in the figure. Streaking of the diffraction peaks along the stacking direction is clearly seen in panel (a) indicating the presence of layer stacking disorder.

dx.doi.org/10.1021/ic202066n | *Inorg. Chem.* 2012, 51, 557–565

(2a) and ordered (2b) variants of Cu_5SbO_6. It is immediately apparent that the ordered variant displays sharp electron diffraction spots, while the disordered one shows the presence of lines of strongly streaked peaks in the reciprocal lattice direction perpendicular to the honeycomb layers, a strong and unambiguous proof of stacking disorder of the planes.

The detailed structural analysis was performed on the ordered stacking phase, because in an X-ray diffraction measurement of the average structure the lack of long-range order between the layers in the disordered form effectively averages the positions of the Sb(V) and Cu(II) cations in the honeycomb, therefore preventing the acquisition of structural information to the precision desired to investigate the possibility of magneto-structural coupling. To obtain a structural model for the ordered variant that is sufficiently high in quality to answer questions about such possible coupling, accommodation had to be made in its observed synchrotron X-ray diffraction pattern for the presence of the disordered variant.

Thus, as a first step, the XRPD pattern of the disordered variant had to be modeled precisely so that its impact on the detailed refinements of the ordered variant could be accommodated. Since this faulted phase is a minor "impurity" in the high temperature ordered phase, and the determination of its average crystal structure is not useful for current purposes, the XRPD data set for the disordered variant was analyzed by a Le Bail profile fit.[24] The characteristic diffraction pattern for the disordered variant was accurately modeled using an orthorhombic unit cell with dimensions of a = 2. 97450(3) Å, b = 5. 59209(6) Å, and c = 11. 51660(13) Å, and the *Pbnn* (#52) space group (Figure 3a). To model the severe peak broadening for this faulted phase, we employed a phenomenological model that describes the broadening of the peaks by a linear combination of ninth order spherical harmonics (SPH).[26,27] This model is implemented in the Rietveld code of the FullPprof program, allowing the treatment to account for the anisotropic size-like broadening in terms of refinable real spherical harmonics coefficients that contribute to the Lorentzian component of the Voigt function employed. Although this has been used to model the broadening caused by stacking faults,[28] the SPH approach is too general to treat strong anisotropic broadening. To employ the diffraction data for the disordered variant quantitatively, a reference mixture (80 wt % disordered variant and 20 wt % α-Al_2O_3) was analyzed. Using the measured intensities on this sample, a refinement was carried out of the relative proportion of the phases until the known proportion was reproduced. This allows the values of the structure factors for the disordered phase to be determined in absolute units.[29] In this refinement, the scale factor of the disordered phase was refined by assuming the composition Cu_5SbO_6 for the disordered variant and keeping the relative intensities constant. Other parameters, such as cell parameters, profile shape, global temperature factor, and asymmetry were also refined. α-Al_2O_3 was treated in the normal fashion. The fit obtained provides the structural information contained in the *hkl* integrated intensities as well as the microstructural information that is included in the peak shape.[29] The structure factors were then used to model the integrated intensities of the disordered variant in the sample of the ordered variant that was analyzed quantitatively; the quantitative contribution of the disordered phase to the diffraction pattern of the high temperature ordered variant (see below) could therefore be estimated. Because we are concerned

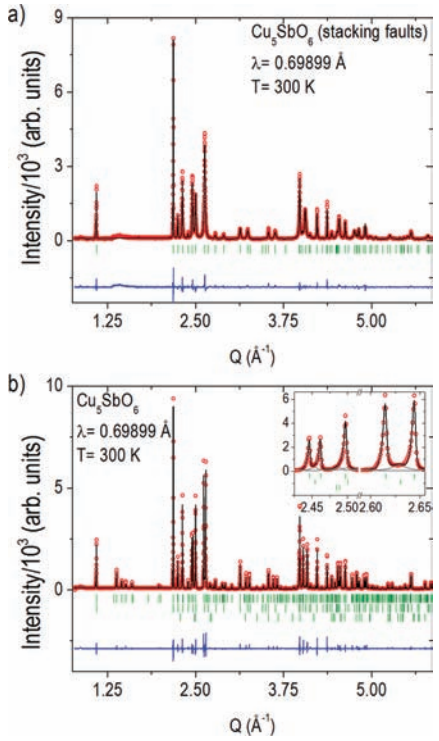

Figure 3. Observed (open circles), calculated (solid line), and difference (lower solid line) high resolution synchrotron XRPD profiles for the disordered (a) and ordered (b) variants of Cu_5SbO_6 at 300 K. The upper panel shows one set of tick marks that indicates the calculated Bragg positions (Le Bail method) for the disordered form. The lower panel, showing the data on which the quantitative structural analysis (Rietveld refinement) is based, shows three sets of tick marks. The upper and middle rows of tick marks show the Bragg positions for the ordered and disordered forms of Cu_5SbO_6, respectively, while the third row shows the calculated positions for CuO. The inset in the lower panel shows the part of the diffraction pattern clearly affected by the presence of small quantities of the disordered variant and CuO in the ordered variant.

only with accommodating the presence of the relatively weak diffraction from the disordered "impurity" in the diffraction pattern of the ordered variant, this approach works very well.

The crystal structure of Cu_5SbO_6 in its ordered stacking phase was found from the structure refinements to be monoclinic, $C2/c$ space group (#15), with unit cell parameters at 300 K a = 8.92346(3) Å, b = 5.592776(16) Å, c = 11.84459(4) Å, and β = 103.58453(17)°. The final fitted synchrotron XRPD pattern at 300 K for the ordered variant of Cu_5SbO_6 is shown in Figure 3b; the figure shows the excellent fit of the data by the structural model. There is no overall change in symmetry of the structure between 300 and 20 K, and therefore a similar fit to the low temperature synchrotron XRPD data, obtained at 20 K, was also performed. The refined structural parameters at 300 and 20 K are presented in Table 1. The inset in Figure 3b shows details of regions in the diffraction pattern from the ordered variant where the presence of the disordered variant and the CuO impurity (this sample was synthesized with an excess of CuO, as described) are the most pronounced. Inspection of the region near Q = 2.63 $Å^{-1}$ shows the presence of a small and broad peak from the disordered variant (middle set of tick marks) between two peaks from the ordered variant. The phase content of this disordered variant

dx.doi.org/10.1021/ic202066n | *Inorg. Chem.* 2012, 51, 557–565

Table 1. Refined Lattice Parameters, Atomic Positions, and Overall Debye-Waller Factor (B_{ov}) of the Ordered Cu_5SbO_6 in Monoclinic $C2/c$ ($Z = 4$) at 300 and 20 K[a]

				T (K)	
				300	20
a (Å)				8.92346(3)	8.90920(3)
b (Å)				5.592776(16)	5.585598(18)
c (Å)				11.84459(4)	11.84986(4)
β (deg.)				103.58453(17)	103.6007(3)
V (Å^3)				574.590(3)	573.151(3)
O(1)	O^{2-}	8*f*: *x*,*y*,*z*	*x*	0.6164(12)	0.6185(13)
			y	0.3762(15)	0.3809(16)
			z	0.5964(9)	0.5955(11)
O(2)	O^{2-}	8*f*: *x*,*y*,*z*	*x*	0.2215(12)	0.2236(13)
			y	0.9280(16)	0.9165(19)
			z	0.9182(8)	0.9120(10)
O(3)	O^{2-}	8*f*: *x*,*y*,*z*	*x*	0.4473(13)	0.4523(12)
			y	0.1192(17)	0.1178(18)
			z	0.0913(10)	0.1009(10)
Cu(1)	Cu^{+}	8*f*: *x*,*y*,*z*	*x*	0.4165(2)	0.4166(3)
			y	0.7494(5)	0.7499(8)
			z	0.0021(2)	0.0012(2)
Cu(2)	Cu^{2+}	8*f*: *x*,*y*,*z*	*x*	0.8281(3)	0.8298(3)
			y	0.0953(3)	0.0991(3)
			z	0.2422(2)	0.2449(2)
Cu(3)	Cu^{2+}	4*e*: 0,*y*,1/4	*y*	0.6292(5)	0.6220(5)
Sb(1)	Sb^{5+}	4*c*: 3/4,3/4,0			
B_{ov} (Å^2)				0.112(18)	0.071(22)
R_{Bragg} (%)				3.36	6.58
R_P (%)				7.49	11.2
wR_P (%)				10.1	14.6
χ^2				11.00	8.30

[a]Agreement factors (R_{Bragg}, R_P, wR_P, and χ^2) are also given.

was found to be at approximately the 20 wt % level. The region of the pattern near $Q = 2.48$ Å^{-1} similarly shows the presence of a small amount (3 wt %) of CuO (bottom tick marks). Figure 4 shows a HREM image that presents a real space confirmation of the stacking order in the ordered variant. The lines of white spots of medium intensity aligned at the β angle of ~103 degrees from the dominant horizontal lines of spots show a region of monoclinic stacking. This monoclinic stacking was observed to be followed regularly over large parts of the sample, not shown in this figure. An image simulation was done with the refined structural model from the synchrotron XRPD data at 300 K (Table 1), shown on the left for the monoclinic stacking. A good fit is obtained between the experimental and simulated images.

To investigate the stacking disorder further, DIFFaX modeling was performed using the layer structure determined from the Rietveld refinement of the ordered Cu_5SbO_6 structure. A double layer was described in an orthorhombic unit cell related to the monoclinic unit cell as $a_O = a_M$, $b_O = b_M$, $c_O = c_M \times \sin \beta$. The monoclinic symmetry was obtained by using one stacking vector ($c_M \times \cos \beta/a_M$, 0, 1). The disordered structure was calculated using the same structural element, but with a 50% stacking probability for each of the vectors ($c_M \times \cos \beta/a_M$, 0, 1) and ($-c_M \times \cos \beta/a_M$, 0, 1). Figure 5 shows the DIFFaX-simulated and observed X-ray diffraction patterns using disordered (Figure 5a) and ordered stacking (Figure 5b). A rather good agreement is seen between position, intensity,

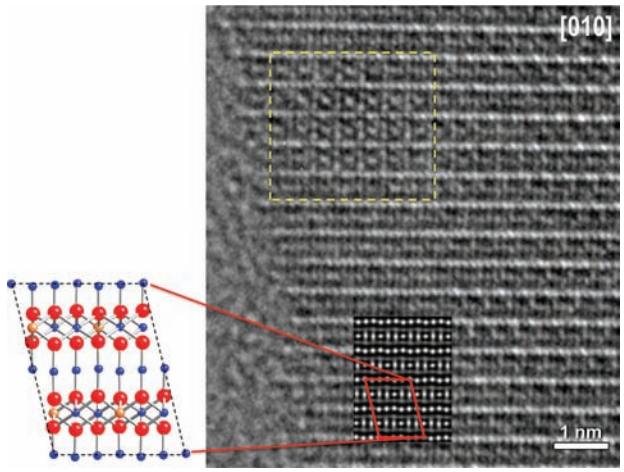

Figure 4. HRTEM image of Cu_5SbO_6 presenting a real space confirmation of the stacking order in the ordered variant. In the highlighted part, the lines of medium intensity white spots are aligned at the β angle of ~103 degrees from the dominant horizontal lines of spots. This monoclinic stacking was observed also over a larger part, not shown in this figure. Image simulation ($E = 300$ kV, $C_S = 0$, convergence 0.15 mrad, focus spread 5 nm, defocus $\Delta f = +5$ nm, mechanical vibration 0.03 nm, and thickness $t = 4$ nm) was done by using the model shown on the left for the ordered monoclinic stacking (large blue circles, Cu, large green circles, Sb, large red circles). The dashed-yellow square shows the presence of disordered regions in the ordered variant.

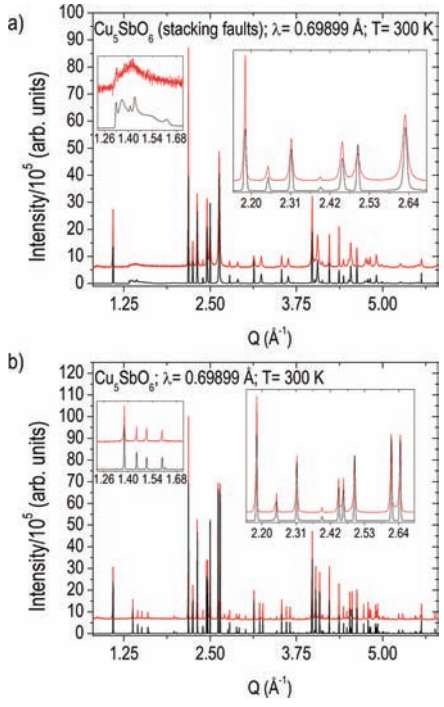

Figure 5. High resolution synchrotron XRPD patterns and DIFFaX simulations for the disordered (upper panel) and ordered (lower panel) variants of Cu_5SbO_6 at 300 K. Raw data and simulated curves are shown as red and black solid lines, respectively. The insets in the upper and lower panels show the parts of the diffraction patterns most affected by the disorder.

anisotropic line broadening, and discontinuities observed in the disordered phase. Notice especially the reproduction of the broad feature between $Q = 1.3$ and 1.6 Å^{-1}, and the disappearance of the ordered-phase peak-splitting at a Q value of about 2.45 and 2.64 Å^{-1}. Although the powder diffraction

dx.doi.org/10.1021/ic202066n | Inorg. Chem. 2012, 51, 557–565

pattern of the disordered phase is not fully reproduced using this simple model, the good agreement confirms the structure as a heavily disordered modification of the monoclinic ordered phase. The electron microscopy images show that the disordered phase can be understood in terms of the presence of disordered regions within the ordered structure, rather than in terms of a discrete phase, as can be seen in the small yellow square in Figure 4.

Figure 6 shows the crystal structure of Cu_5SbO_6. Figure 6a shows the geometry of the honeycomb Cu_2SbO_6 layer, which is

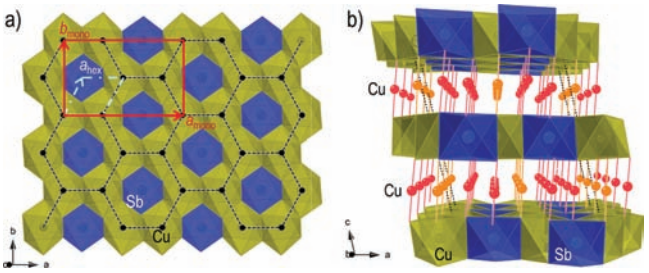

Figure 6. Delafossite honeycomb crystal structure of Cu_5SbO_6. (a) View perpendicular to the honeycomb layer with the Cu^{2+} honeycomb arrangement emphasized (black dashed lines and dots). $Sb(V)O_6$ octahedra are shown in blue (dark) while $Cu(II)O_6$ octahedra are shown in yellow (light). A schematic illustration of the relationship of the unit cell axes between the hexagonal (light-gray dashed-dot arrows) and monoclinic (red solid arrows) cells is also included. (b) View parallel to the honeycomb layers. The two types of O−Cu(I)−O sticks that separate the planes are shown, and the unit cell is shown by black dotted lines.

made from Cu^{2+} and Sb^{5+} (Cu(1) and Sb(1), located on 8*f* and 4*c* sites in Table 1) octahedra sharing edges in a 2:1 ratio. The Cu^{2+} honeycomb lattice is emphasized. The Cu^{2+} and Sb^{5+} ions are coplanar, but do not form an ideal equilateral triangle lattice geometry. The close packed layers of oxygen (O(1), O(2), and O(3) located on 8*f* sites in Table 1) above and below the metal plane are irregular in shape and slightly puckered, accommodating the Jahn−Teller (J-T) distortion of the $3d^9$ Cu^{2+} ions, as described below. The crystallographic monoclinic unit cell in this plane, shown in the figure by red solid lines, deviates from the ideal pseudohexagonal plane ($a_{hex} \sim b_{hex} \sim 3.1$ Å) where $a_{mono} \approx 3a_{hex}$, $b_{mono} \approx \sqrt{3}a_{hex}$, shown in the figure by light-gray dashed lines, by a shortening of ~8% along *a* because of the Cu−O J-T distortion. Figure 6b shows the stacking of the layers. Cu^+ ($3d^{10}$) ions in the expected stick geometry are found between planes, connecting all oxygens in the honeycomb planes above and below. The cell symmetry dictates that there are two independent Cu^+ ions (Cu(2) and Cu(3) located on 8*f* and 4*e* in Table 1) in these spacer layers, in a 2:1 ratio; all connect honeycomb plane oxygens that are shared by two $Cu(II)O_6$ octahedra and one $Sb(V)O_6$ octahedron. The monoclinic cell, with a β angle of ~103.58 degrees, is shown by the dotted line. Given the J-T distortion that always accompanies Cu^{2+} in octahedral geometry, and the required accompanying distortion in the shape of the honeycomb plane, an ideal hexagonal or rhombohedral symmetry structure is not possible for Cu_5SbO_6. Thus, the lower symmetry allows the structure to relax. The stacking of several layers of the honeycomb, abstracted to their simple form for the metal atoms in the honeycomb only, is presented in Figure 7a and b. The figure shows that the honeycomb metal layers are staggered, not eclipsed, in a fashion that repeats after 1.5 cells,

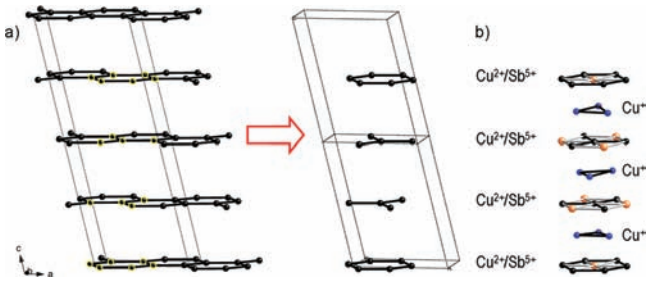

Figure 7. (a) Schematic view of arrangement of the metal atoms in the honeycombs in Cu_5SbO_6 when viewed in a direction parallel to the layers. (b) The honeycombs are staggered, and the layer sequence repeats after 3 translations making this, if considering the metal atoms in the honeycomb layer only, effectively a pseudo-3R Delafossite structure.

forming a pseudo 3R-polytype honeycomb RMO_2 Delafossite compound. An ideal 3R polytype has been reported for the related compound $Cu_3Ni_2SbO_6$ where the effects of the J-T distortion are not present.[11]

A selection of chemically relevant bond angles and distances at room temperature and 20 K is presented in Table 2. All

Table 2. Selected Bond Distances (Å) and Angles (deg.) Found for Cu_5SbO_6 from the Rietveld Analysis of the XRPD Data at 300 and 20 K[a]

		T (K)	
		300	20
Cu	d_{ax}	2.309(14)	2.335(10)
		2.376(11)	2.350(9)
	d_{eq}	1.968(12)	1.968(12)
		1.984(10)	1.986(11)
		1.996(10)	1.990(12)
		2.050(10)	2.039(10)
	Θ_{ax}	177.9(3)	179.2(4)
	Θ_{eq}	171.2(4), 171.1(4)	172.5(5), 173.8(5)
	Θ_{hc1},Θ_{hc2},Θ_{hc3}	92.6(4), 93.9(5), 95.8(4)	93.4(4), 92.7(5), 93.13(9)
	Δ_d	0.595	0.566
		1.103[b]	
		1.400[c]	
	d_{hc1}	2.960(3)	2.946(3)
	d_{hc2}	3.169(4)	3.170(5)
		3.181(4)	3.179(5)
Sb	d_{ax}	2.032(9) × 2	2.100(10) × 2
	d_{eq}	1.966(12) × 2	2.003(10) × 2
		1.978(13) × 2	2.007(10) × 2
	Δ_d[d]	0.021	0.048
		0.050[b]	
		0.026(Te)[c]	

[a] d_{ax} (×2) and d_{eq} (×4) denote the local axial and equatorial Cu(1)−O and Sb(1)−O bond lengths in the octahedra. Θ_{ax} and Θ_{eq} (×2) indicate the local axial and equatorial O−Cu(1)−O bond angles in the octahedra. d_{hc1} and d_{hc2} (×2), and Θ_{hc1}, Θ_{hc2}, and Θ_{hc3} indicate the Cu(1)−Cu(1) bond distances and Cu(1)−O(1,2,3)-Cu(1) bond angles in the honeycomb layers, respectively. The mean square deviations from ideal octahedral symmetry (Δ_d, %) are also included. [b]And $Na_3Cu_2TeO_6$. [c]Ref 6, 7. [d]$\Delta_d = (1/6)\sum_{n=1,6}[(d_n - \langle d\rangle)/\langle d\rangle]^2 \times 100$; Δ_d's for $Na_3Cu_2SbO_6$.

Cu−O bond lengths are as expected (1.96−2.40 Å) and nearly equivalent at the two temperatures. The $Cu(II)O_6$ octahedra are distorted, again as expected, with a J-T distortion

dx.doi.org/10.1021/ic202066n | *Inorg. Chem.* 2012, 51, 557−565

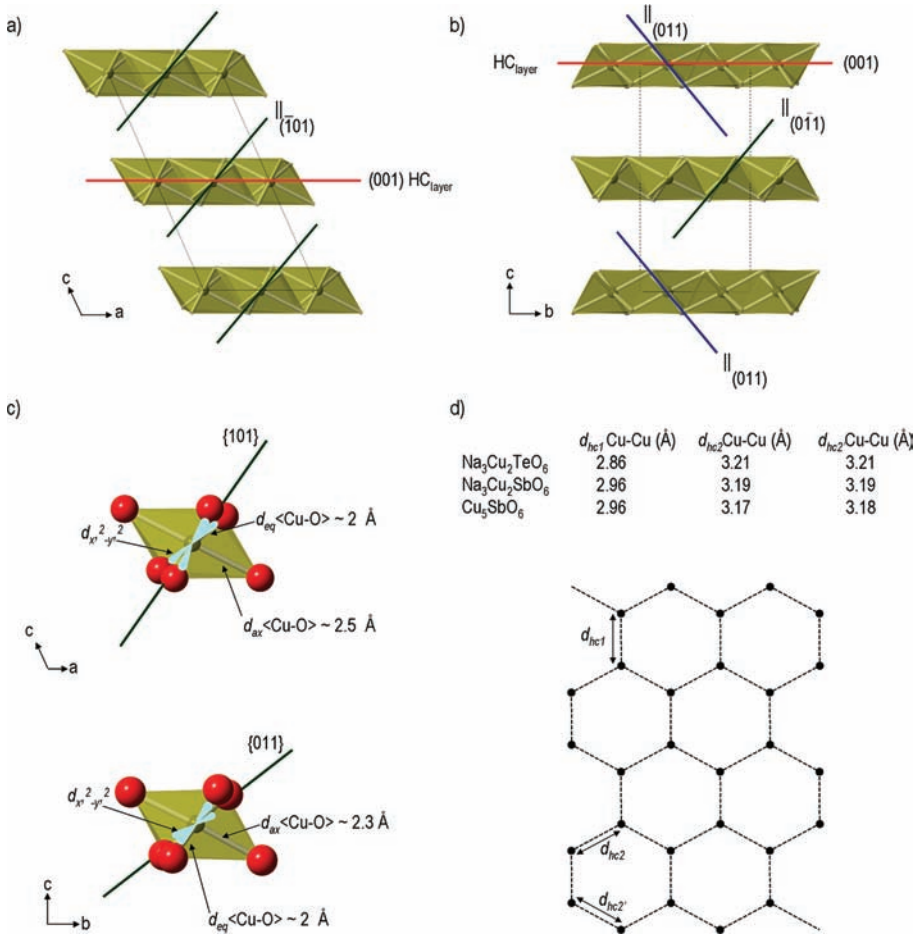

Figure 8. Important structural characteristics of Cu_5SbO_6 compared to those in $Na_3Cu_2SbO_6$ and $Na_2Cu_2TeO_6$ (5,6). In panels a–c, the brown and blue solid lines denote the orientations of the Cu $d_{x^2-y^2}$ orbital planes in the J-T distorted octahedra. (a and b) The honeycomb planes, with the Cu–O octahedra fully rendered. Within the individual layers, all the Cu $d_{x^2-y^2}$ orbital planes are aligned. In $NaFeO_2$-derived $Na_2Cu_2TeO_6$ and $Na_3Cu_2SbO_6$, (a), the $d_{x^2-y^2}$ orbital planes are parallel in all the layers, while in Delafossite-derived Cu_5SbO_6, (b), the $d_{x^2-y^2}$ orbital planes in adjacent layers are approximately perpendicular. (c) The relative sizes, shapes, and orientations of the Cu(II)O_6 octahedra in $Na_3Cu_2(Te,Sb)O_6$ (upper) and Cu_5SbO_6 (lower). (d) Schematic comparison of the Cu^{2+} honeycomb lattices for the three compounds, with the Cu–Cu distances tabulated.

characterized by average $d_{z'^2}$ (z' indicates a local octahedron axis) and $d_{x'^2-y'^2}$ (x' and y' indicate local octahedron axes) bond lengths of ~2.34 and ~2.00 Å, respectively. The Sb(V)O_6 octahedra are also slightly distorted no doubt to accommodate the Cu^{2+}, with bond lengths varying from ~2.03 to ~1.98 Å. Employing the expression for the mean square deviation from ideal octahedral symmetry often employed to describe such distortions in perovskites,[30] we find mean square deviations of $\Delta_d \sim 0.6\%$ for the Cu(II)O_6 octahedra and $\Delta_d \sim 0.02\%$ for the Sb(V)O_6 octahedra. The deviations for the Cu(II) are much lower than is seen for the Cu(II) in the $NaFeO_2$-like honeycomb compounds $Na_3Cu_2SbO_6$ and $Na_2Cu_2TeO_6$, where they are 1.1% and 1.4%, respectively.

A comparison of several important aspects of the structures of $Na_2Cu_2TeO_6$, $Na_3Cu_2SbO_6$, and Cu_5SbO_6 is shown in Figure 8. Figures 8a ($Na_2Cu_2TeO_6$, $Na_3Cu_2SbO_6$) and 8b (Cu_5SbO_6) show only the honeycomb planes, with the Cu–O octahedra fully rendered. The solid lines mark the orientations of the Cu $d_{x^2-y^2}$ orbital planes in the J-T distorted octahedra within the layers. Within an individual layer in both structure types, all the Cu $d_{x^2-y^2}$ orbital planes and thus the J-T elongations are aligned. When considering adjacent layers, however, there is a major difference between $NaFeO_2$-derived $Na_2Cu_2TeO_6$ and $Na_3Cu_2SbO_6$ and Delafossite-derived Cu_5SbO_6: In the former case (8a) the $d_{x^2-y^2}$ orbital planes are all parallel, while in the later case (8b) they are approximately perpendicular. This may result in subtle differences in the magnetic coupling between layers in the two families of compounds. A comparison of the shapes of the Cu(II)O_6 octahedra in $Na_2Cu_2TeO_6$, $Na_3Cu_2SbO_6$, and Cu_5SbO_6 is also shown in Figure 8c. The J-T distortions are large and very similar in the $NaFeO_2$-derived phases, while in Delafossite-derived Cu_5SbO_6 the J-T distortion is considerably weaker.

For the purpose of understanding the magnetism of Cu_5SbO_6 and the $NaFeO_2$-derived Cu honeycomb phases, several interatomic distances involving the Cu ions are of interest. These distances are shown in the context of the honeycomb lattice in Figure 8d. In all three compounds, two pairs of the Cu in the six-membered rings are substantially closer to each other than would be present for a uniform ring. These are the Cu dimers that form the magnetic singlet state. These dimers repeat in a triangular lattice, but the relative orientations of the dimers do not result in a 3 or 3*m* in-plane symmetry; rather the in-plane symmetry is 2*mm*. The degree of the Cu–Cu dimerization can be easily seen in the difference in separations between the closest Cu's in the ring and the average Cu separation in the ring; the dimerization is larger in the $NaFeO_2$-derived honeycomb phases than in the honeycomb

dx.doi.org/10.1021/ic202066n | *Inorg. Chem.* 2012, 51, 557–565

Delafossite. In $Na_2Cu_2TeO_6$ this difference is $|2.8584 - (2.8584 + 2 \times 3.2136)/3| = 0.2368$ Å, in $Na_3Cu_2SbO_6$ it is $|2.9559 - (2.9559 + 2 \times 3.1993)/3| = 0.1623$ Å, and in Cu_5SbO_6 it is slightly lower, at $|2.9602 - (2.9602 + 3.1686 + 3.1805)/3| = 0.1429$ Å. Thus, while Cu_5SbO_6 has the weakest dimerization at ambient temperature of the three known honeycomb phases, the dimerization is still significant, as can be seen in the deviation from the ideal hexagonal symmetry $a_{mono}/(\sqrt{3}b_{mono}) = 0.921$. This excludes Cu_5SbO_6 as being a good example of an ideal spin $^1/_2$ honeycomb lattice, which is expected to display interesting quantum magnetism because of a resonating valence bond state.[31]

The weaker Cu−Cu dimerization in the honeycomb in Cu_5SbO_6 motivated us to determine the crystal structure of the phase to high precision well below the transition to the fully localized magnetic singlet state (see next section) to determine whether there is any subtle magnetostructural coupling present, that is, whether there is an increasing Peierls-like structural distortion on the honeycomb lattice when the singlet state is fully formed. The results of the low temperature refinement showed that the degree of dimerization changed from |0.1429| Å at room temperature to |0.1395| Å at 20 K. This difference is very small, approximately at the experimental precision, though it is in the expected direction if the dimer does become stronger on cooling through the singlet formation temperature. Thus, any magnetostructural changes that might accompany the development of the full singlet state in Cu_5SbO_6 are very weak, if present.

Magnetic Properties. The temperature dependent magnetic susceptibilities for the ordered and disordered variants of Cu_5SbO_6 between 300 and 2 K are shown in Figure 9. The data have been fitted with the expression for a dimer and a Curie−Weiss term for the impurity ions assumed to be "free" Cu^{2+} ions:

$$\chi = C1/T(3 + \exp(\delta/T)) + C2/(T - \theta) + C3 \quad (1)$$

Where χ is taken as $M/(\mu_0 H)$ at 0.5 T (M vs $\mu_0 H$ is linear in field up to the measurement field of 0.5 T at all temperatures), C1 is the Curie Constant for the bulk spins, δ is the value of the spin gap for excitations of the dimers from the singlet to paramagnetic state, C2 is the Curie Constant for the impurity spins, θ is their Curie−Weiss temperature, and C3 is a temperature independent term. C3 = 0 within error for all samples and was omitted from the final fits. Data are shown in Figure 9a for one sample of the disordered variant of Cu_5SbO_6, and for one sample of the ordered variant (the sample with approximately 20 wt % disordered variant as an "impurity" phase) in Figure 9b. The crystal structure analysis shows one Cu−Cu dimer per formula unit of Cu_5SbO_6 (i.e., $Cu^{1+}{}_3Cu^{2+}{}_2SbO_6$). The value of C1 then contains only one adjustable parameter, namely, the g-factor for Cu. C2 allows for the determination of the concentration of "free" Cu ions/formula unit, that is, those not locked into the singlet state through dimerization because of defects in the crystal structure (we assume $g = 2$ and $S = 1/2$ for the "free" Cu spins). The fits to the data yield, for the disordered variant: $\delta = 191$ K and $g = 2.05$ for the bulk spins, and 2.2% "free" Cu ions with $\theta = -6.6$ K. For the ordered variant, we find $\delta = 186$ K and $g = 2.09$ for the bulk spins, and 2.9% free Cu ions, with $\theta = -0.8$ K. The data are well described by the simple dimer model as shown in Figure 8; the origin of the relatively high θ for the impurity spins in the disordered variant is not currently known. The similar percentages of "free spins" for both variants

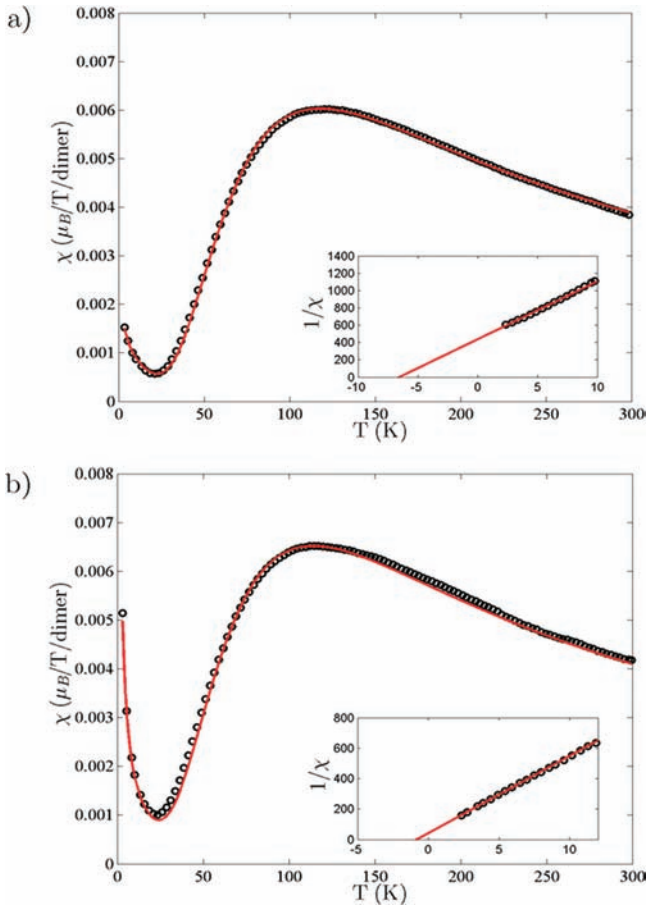

Figure 9. Magnetic susceptibilities measured by VSM at a field of 0.5 T in the temperature range between 2 and 300 K. Open circles are experimental data, the lines are fits using $\chi = C1/T(3 + \exp(\delta/T)) + C2/(T - \theta) + C3$, the dimer susceptibility plus a low temperature Curie−Weiss susceptibility for "free" impurity ions, assumed to be Cu^{2+}. C1 is the Curie Constant for the bulk spins from which we derive g, δ is the value of the spin gap, C2 is the Curie Constant for the impurity spins, and θ is their Curie−Weiss temperature. C3 = 0 within error for all samples. For the disordered variant: $\delta = 191$ K and $g = 2.05$ for the bulk spins, and there are 2.2% "free" Cu ions with $\theta = -6.6$ K. For the ordered variant: $\delta = 186$ K and $g = 2.09$ for the bulk spins, and there are 2.9% free Cu ions, with $\theta = -0.8$ K. The fits for the disordered and ordered samples are shown in panels (a) and (b), respectively. The insets show the inverse susceptibility at low temperatures verifying the Curie−Weiss behavior of the impurity spins.

indicate that the stacking faults do not affect the perfection of the Cu/Sb ordering in the honeycomb layers. The g values obtained are within two standard deviations of that determined from the EPR measurements, where $g = 2.18$ for both variants of the phase.

The temperature dependence of the specific heats for Cu_5SbO_6 and the nonmagnetic analogue Cu_3ZnSbO_6 are shown in Figure 10. Comparison of the data shows the presence of excess specific heat in Cu_5SbO_6 arising from the magnetic entropy released because of the localization of the Cu spins in the Cu−Cu dimers in the temperature range around 100 K. Subtraction of the specific heat for Cu_3ZnSbO_6 from that observed for Cu_5SbO_6 and then integrating in the usual fashion to obtain the magnetic entropy released as a function of temperature yields the plot shown in the inset to Figure 10. The data shows the release of entropy in

dx.doi.org/10.1021/ic202066n | Inorg. Chem. 2012, 51, 557−565

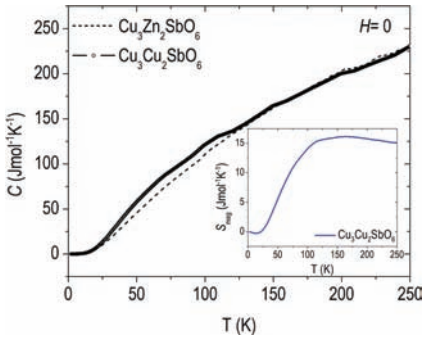

Figure 10. Main panel, the temperature dependent specific heats for the ordered variant of Cu_5SbO_6 and for the nonmagnetic analogue $Cu_3Zn_2SbO_6$. Comparison of the data show the presence of specific heat in excess of that due to phonons for Cu_5SbO_6. The excess specific heat is released in the temperature range of 25−125 K. The inset shows the integrated entropy released, obtained from $\Delta S = \int [C_p(Cu_5SbO_6) - C_p(Cu_3Zn_2SbO_6)]/T\ dT$.

the expected fashion in the temperature range expected from the magnetic susceptibility. The total entropy released, about 15 J/(mol K), is larger than that expected for 2 Cu per formula unit each releasing R ln 2 J/K, which would be about 11.5 J/(mol K). This suggests that there may be entropy in excess of that due to magnetism alone released in the formation of the singlet state in Cu_5SbO_6, a possible indication of subtle structural or vibrational changes accompanying the formation of the singlet state.

4. CONCLUSIONS

Cu_5SbO_6 is found to display a Delafossite-derived crystal structure with the 2:1 ordering of Cu^{2+} and Sb^{5+} in edge sharing octahedra in the triangular metal planes resulting in a magnetic Cu^{2+} honeycomb geometry. Strong Jahn−Teller distortions of the Cu(II)O_6 octahedra are present, resulting in the monoclinic overall symmetry, and the formation of Cu^{2+}−Cu^{2+} dimers. The dimers form in a dimensionally triangular lattice, but their relative orientations make the in-plane lattice rectangular rather than triangular. The structural dimers lead to the observation of the classic temperature dependent magnetic susceptibility for a dimerized system in which the ground state is a spin singlet. Thus, the susceptibility data for temperatures up to 300 K can be modeled in detail by considering only a single antiferromagnetic interaction forming the singlet−triplet state with an energy gap of about 189 K. Further studies of the magnetic properties are of interest. The very similar nature of the magnetic susceptibilities for the ordered and disordered stacking variants of the phase indicates that the magnetism is highly dominated by the magnetism due to the dimers and that any influence of interplanar coupling must be very small. Comparison to the previously known $NaFeO_2$-derived Cu^{2+} honeycomb compounds $Na_2Cu_2TeO_6$ and $Na_3Cu_2SbO_6$ reveals significant structural differences, but these differences do not appear to be significant enough to change the basic magnetic properties. A hint of magnetostructural coupling resulting from the low temperature singlet formation is found in the comparison of the low and high temperature structures of Cu_5SbO_6, but it is comparable to the precision of the measurements; this possibility is also suggested in the analysis of the entropy released during the singlet formation. Continuing search for compounds displaying Cu^{2+} honeycomb lattices, and the possibility that they might display predicted resonating valence bond physics,[31] should be of significant future interest.

AUTHOR INFORMATION

Corresponding Author

*E-mail: ecliment@princeton.edu.

ACKNOWLEDGMENTS

The work at Princeton was supported by the Department of Energy, Division of basic Energy Sciences, Grant DE-FG02-08ER46544. Use of the National Synchrotron Light Source, Brookhaven National Laboratory, was supported by the U.S. Department of Energy, Office of Science, Office of Basic Energy Sciences, under Contract No. DE-AC02-98CH10886. R.J.C. gratefully acknowledges the support for his work at Risø DTU by the Velux Visiting Professor Program 2009-2010. We also thank Dr. Carlos Pacheco (Department of Chemistry, Princeton University) for his assistance in performing the EPR measurements.

REFERENCES

(1) Lacroix, C.; Mendels, P.; Mila, F. *Introduction to Frustrated Magnetism: Materials, Experiments and Theory*; Springer-Verlag: Berlin, Germany, 2011.
(2) Yamashita, S.; Moriura, T.; Nakazawa, Y.; Yoshida, H.; Okamoto, Y.; Hiroi, Z. *J. Phys. Soc. Jpn.* **2010**, *79*, 083710.
(3) Helton, J. S.; Matan, K.; Shores, M. P.; Nytko, E. A.; Bartlett, B. M.; Yoshida, Y.; Takano, Y.; Suslov, A.; Qiu, Y.; Chung, J.-H.; Nocera, D. G.; Lee, Y. S. *Phys. Rev. Lett.* **2007**, *98*, 107204.
(4) Regnault, L. P.; Rossat-Mignod, J. *Magnetic Properties of Layered Transition Metal Compounds*; Kluwer Academic Pub: Dortrecht, The Netherlands, 1989.
(5) Smirnova, O.; Azuma, M.; Kumada, N.; Kusano, Y.; Matsuda, M.; Shimakawa, Y.; Takei, T.; Yonesaki, Y.; Kinomura, N. *J. Am. Chem. Soc.* **2009**, *131*, 8313.
(6) Xu, J.; Assoud, A.; Soheilnia, N.; Derakhshan, S.; Cuthbert, H. L.; Greedan, J. E.; Whangbo, M. H.; Kleinke, H. *Inorg. Chem.* **2005**, *44*, 5042.
(7) Smirnova, O. A.; Nalbandyan, V. B.; Petrenko, A. A.; Avdeev, M. *J. Solid State Chem.* **2005**, *178*, 1165.
(8) Kol'tsova, T. N.; Chastukhin, A. E. *Inorg. Mater.* **2002**, *38*, 1228.
(9) Shimada, S.; Mackenzie, K. J. D. *Thermochim. Acta.* **1982**, *56*, 73.
(10) Shimada, S.; Mackenzie, K. J. D.; Kodaira, K.; Matsushita, T.; Ishii, T. *Thermochim. Acta* **1988**, *73*, 133.
(11) Stan, M.; Mihaiu, S.; Crisan, D.; Zaharescu, M. *Eur. J. Solid State Inorg. Chem.* **1998**, *35*, 243.
(12) Nagarajan, R.; Uma, S.; Jayaraj, M. K.; Tate, J.; Sleight, A. W. *Solid State Sci.* **2002**, *4*, 787.
(13) Hosogi, Y.; Kato, H.; Kudo, A. *J. Mater. Chem.* **2008**, *18*, 647.
(14) Politaev, V. V.; Nalbandyan, V. B.; Petrenko, A. A.; Shukaev, I. L.; Volotchaev, V. A.; Medvedev, B. S. *J. Solid State Chem.* **2010**, *183*, 684.
(15) O'Malley, M. J.; Verweij, H.; Woodward, P. M. *J. Solid State Chem.* **2008**, *181*, 1803.
(16) Kobayashi, H.; Kanno, R.; Kawamato, Y.; Tabuchi, M.; Nakamura, O.; Takano, M. *Solid State Ionics* **1995**, *82*, 25.
(17) Kimber, S. A. J.; Ling, C. D.; Morris, D. J. P.; Chemseddine, A.; Henry, P. F.; Argyriou, D. N. *J. Mater. Chem.* **2010**, *20*, 8021.
(18) Ingram, B. J.; González, G. B.; Mason, T. O.; Shahriari, D. Y.; Barnabe, A.; Ko, D.; Poeppelmeier, K. R. *Chem. Mater.* **2004**, *16*, 5616.
(19) Isawa, K.; Yaegashi, Y.; Komatsu, M.; Nagano, M.; Sudo, S.; Karppinen, M.; Yamauchi, H. *Phys. Rev. B* **1997**, *56*, 3457.
(20) Louër, D.; Louër, M. *J. Appl. Crystallogr.* **1972**, *5*, 271.
(21) Boultif, A.; Louër, D. *J. Appl. Crystallogr.* **2004**, *37*, 724.
(22) Favre-Nicolin, V.; Černý, R. *J. Appl. Crystallogr.* **2002**, *35*, 734.
(23) Rodríguez-Carvajal, J.; Roisnel, T. *FullProf, WinPLOTR*, and accompanying programs; 2008; http://www.ill.eu/sites/fullprof/index.html (accessed January 2011).
(24) Treacy, M. M. J.; Newsam, M. J.; Deem, M. W. *Proc. R. Soc. A* **1991**, *433*, 499.

(25) Le Bail, A.; Duroy, H.; Fourquet, J. L. *Mater. Res. Bull.* **1988**, *23*, 447.
(26) Popa, N. C. *J. Appl. Crystallogr.* **1998**, *31*, 176.
(27) Popa, N. C.; Balzar, D. *J. Appl. Crystallogr.* **2008**, *41*, 615.
(28) Casas-Cabanas, M.; Palacín, M. R.; Rodríguez-Carvajal, J. *Powder Diffr.* **2005**, *20*, 334.
(29) Taylor, J. C.; Rui, Z. *Powder Diffr.* **1992**, *7*, 152.
(30) Alonso, J. A.; Martinez-Lope, M. J.; Casais, M. T.; Fernandez-Diaz, M. T. *Inorg. Chem.* **2000**, *39*, 922.
(31) Banerjee, A.; Damle, K.; Paramekanti, A. arXiv:1012.4546v2, 2010.